

Water Resources Research



RESEARCH ARTICLE

10.1029/2019WR025266

Inference of Retention Time From Tracer Tests in Crystalline Rock

Key Points:

- Tracer tests are the only in situ evidence of retention in granite and hence are important, for example, in the context of geological waste disposal
- Novel methodology is developed and implemented for separating effects of retention and hydrodynamic transport critical for upscaling
- Relating key transport-retention parameters to independent information on material and structural properties of rocks is highly uncertain

Correspondence to:

V. Cvetkovic,
vdc@kth.se

Citation:

Cvetkovic, V., Poteri, A., Selroos, J.-O., & Zou, L. (2020). Inference of retention time from tracer tests in crystalline rock. *Water Resources Research*, 56, e2019WR025266. <https://doi.org/10.1029/2019WR025266>

Received 29 MAR 2019

Accepted 24 JAN 2020

Accepted article online 26 JAN 2020

Vladimir Cvetkovic¹, Antti Poteri², Jan-Olof Selroos³, and Liangchao Zou¹

¹Division of Water Resources Engineering, KTH Royal Institute of Technology, Stockholm, Sweden, ²Posiva Oy, Helsinki, Finland, ³Swedish Nuclear Fuel and Waste Management Co. (SKB), Stockholm, Sweden

Abstract A statistical parametrization of transport combined with a new, general partition function for diffusive mass transfer (Cvetkovic, 2017, <https://doi.org/10.1002/2017WR021187>) is here developed into a practical tool for evaluating tracer tests in crystalline rock. The research question of this study is how to separate the characteristic times of retention and advection, using tracer test information alone; this decoupling is critical for upscaling of transport. Three regimes are identified based on the unconditional mean number of trapping events. Analytical expressions are derived for inferring transport-retention parameters; these are first tested on a series of generic examples and then using two sets of tracer test data. Our results indicate that the key transport-retention parameters can be inferred separately with reasonable accuracy by a few simple steps, provided that the macrodispersion is not too large and retention not too strong. Of particular interest is inference of the retention time from the breakthrough curve peak that avoids costly asymptotic monitoring. Finally, we summarize the retention times as inferred from a series of nonsorbing tracer tests in the Swedish granite, demonstrating the uncertainties when estimating retention based on material and structural properties from samples. Possible strategies for reducing these uncertainties that combine improved understanding of crystalline rock evolution with numerical simulations are noted as topics for future research.

1. Introduction

Experimental studies of tracer retention have been pivotal for developing the concept of geological waste disposal. The original work by Fried et al. (1987) focused on transport and equilibrium sorption of radionuclides Pu and Am for a small basalt rock sample. In analogy to heat exchange from parallel plates, retention in rocks was proposed as a diffusion-controlled exchange combined with equilibrium sorption by Neretnieks (1980). Since the works of Fried et al. (1987) and Neretnieks (1980), numerous theoretical and experimental studies have been carried out to better understand transport and retention in rocks (Cvetkovic, 2010a; Cvetkovic et al., 2007, 2010; Hadermann & Heer, 1996; Haggerty et al., 2000; Heer & Smith, 1998; Johansson et al., 1997, 1998; Ittner et al., 1990; Reimus et al., 2003; Reimus & Callahan, 2007; Robinet et al., 2008; Sardini et al., 2007; Selnert et al., 2007; Shapiro, 2001; Widstrand et al., 2007). One challenge with transport experiments in rocks is that water flow affects retention, yet the flow is often complex and difficult to control or describe in sufficient detail (e.g., Cvetkovic et al., 2007, 2010; Cvetkovic & Frampton, 2010).

A tracer test in sparsely fractured crystalline rock designed to capture transport and retention, will typically combine hydrodynamic (advection-dominated) transport through fractures, and retention due to tracer mass transfer from the mobile water in fractures to the essentially immobile water in the matrix. The design of a tracer test will first consider material retention properties of the rock (mainly porosity and tortuosity in the rim zone of fractures where the mass transfer takes place over the tracer test time scales) and of the tracer (e.g., diffusivity in water and radioactive decay). If the tracer is sorbing then its sorption properties would need to be defined for a particular rock type with its mineralogical composition, and the geochemical composition of groundwater. Next, the structural and hydraulic properties of fractures such as the aperture and transmissivity need to be estimated and taken into account when designing a tracer test. Finally, the boundary conditions for the flow (e.g., the pumping rate) need to be selected in a way that is both practical and will enable retention to sufficiently develop.

Although for idealized conditions we understand the underlying physical and chemical processes that combine above parameters and properties and can test several of them in the laboratory, predicting a tracer test

©2020. The Authors.

This is an open access article under the terms of the Creative Commons Attribution License, which permits use, distribution and reproduction in any medium, provided the original work is properly cited.

outcome based on information about the properties of the tracer and the rock is highly uncertain due to rock heterogeneity, even if the available information is extensive. The tracer test outcome will depend on a number of detailed properties (such as specific channeling and material properties along dominant channels for the flow, depending on the exact location of the boreholes), which in practice cannot be determined with sufficient accuracy independently from the tracer test itself. Thus, the actual outcome of a tracer test (typically as a breakthrough curve [BTC] defined as tracer mass per unit time) over a given duration is ultimately the only reliable evidence of in situ transport and retention. In order to obtain useful information needed for upscaling tracer transport, the main challenge then is to evaluate a tracer test outcome in a way that most reliably separates (or decouples) in situ hydrodynamic transport (which depends on boundary conditions) from material and structural retention properties.

In this work, we address the general problem of characterizing transport and retention in sparsely fractured granitic rocks using tracer tests. The specific issue we wish to resolve is how to decouple (separate) retention from the hydrodynamic information based solely on tracer tests observations. To this end, recently presented theoretical results (Cvetkovic, 2017) are combined with tracer test data to improve our understanding of the fundamental limitations when inferring parameters from tracer tests and propose approximate steps for overcoming these limitations. The retention process is modeled in a general way, without a priori assuming any type of idealized geometry (such as rectangular channels or pipes) for flow paths in fractures; the idealized representation can be recovered as a special case. To fulfil our objectives, three retention regimes for tracer test outcomes are identified with different evaluation strategies proposed for each one; these rely on a statistical description of the mass transfer process with the mean number of immobilization events as a critical parameter.

2. Problem Formulation

Groundwater flow in sparsely fractured crystalline rock takes place through fractures. There is ample evidence that flow in fractures is channelized (e.g., Tsang & Neretnieks, 1998), consequently inert tracer transport tends to be advection dominated. The hydrodynamic component of transport will predominantly take place along channels or flow paths within fractures, which are essentially random due to rough fracture surfaces; these then aggregate into random networks that will dominate tracer transport on larger scales.

From the mobile water in fractures, tracer advection along flow paths will be interrupted by immobilization events where tracer particles become temporarily trapped in the immobile water for a random time, and then returning to the mobile water; such cycles are an expression of mass transfer which in the crystalline rock is diffusion controlled for nonsorbing tracers, and diffusion-sorption controlled for sorbing tracers.

The mass transfer process between the mobile and immobile water in rocks was first described as a first-order exchange process (Coats & Smith, 1964). Subsequent developments were based on Fickian diffusion from idealized rectangular channels (Carslaw & Jaeger, 1959; Neretnieks, 1980) and still later based on analogy with the Reynolds equation for flow, where an idealized geometry is assumed locally (Cvetkovic et al., 1999). Recently, a general mass transfer model was proposed as a truncated power law partition function (Cvetkovic, 2017). This general model does not assume any type of geometrical idealization (globally or locally), and is parametrized by two characteristic times and an exponent, with the exponent taking value $1/2$ if Fickian diffusion in the rock matrix is assumed.

Fundamentally, the hydrodynamic transport (as randomized advection) and mass transfer (as retention) are coupled. When a tracer test is conducted in granite, this coupling is expressed as a parameter group where the primary effect of hydrodynamic transport is quantified by the mean water travel time. For transport upscaling, it is paramount to separate or decouple hydrodynamic transport effects from retention effects, since hydrodynamics depends strongly on boundary conditions for flow, whereas retention does not. In theory, we could separate hydrodynamic transport from the retention effects based on independent information, such as material retention properties (matrix porosity, sorption coefficient, and diffusivity) obtained from samples, or hydraulic and structural information deduced from hydraulic and geophysical tests. Evidence indicates however that the independent information is highly uncertain for verifying in situ tracer tests, calling for improved methods to separate effects of hydrodynamics and retention from tracer test information

The research question addressed in this work is formulated as follows: *How can the hydrodynamic and retention effects expressed as characteristic advection and retention times be separated (decoupled) based solely on information obtained from tracer tests in crystalline rock?*

To answer this question, we develop and implement a methodology with the following key points:

- Advection-retention theory is first formulated with all components that are required for tracer test evaluation, starting from tracer mass balance and ending with a statistical representation of the retention process (section 3).
- Based on the theory, transport-retention is categorized into three different regimes; suitable analytical expressions are derived for each one, with the particular aim of separating hydrodynamic effects in form of mean water travel time from retention effects (section 4).
- The derived expressions for different retention regimes are systematically tested on generic examples (section 5).
- The derived expressions for two different retention regimes are tested against data from two tracer tests (section 6).
- The set of examples is broadened to include eight more tests with nonsorbing tracers in order to emphasize the significance of the physical processes (diffusion and flow) and discuss associated uncertainties (section 7).

3. Theory

The mass balance equations for solute with concentration in mobile phase C [M/L³] and in immobile phase S [M/L³] are written as

$$\frac{\partial C}{\partial t} + \nabla \cdot \mathbf{J} = -F(C, S) ; \quad \frac{\partial S}{\partial t} = F(C, S) \quad (1)$$

where \mathbf{J} [M/TL²] is the solute flux and F [M/TL³] is a sink-source term that quantifies reversible exchange.

The main assumptions are summarized as follows:

1. Solute exchange is linear in a generalized sense of Villermaux (1974), that is, $\widehat{S}/\widehat{C} = \widehat{g}$, where $\widehat{(\cdot)}$ denotes Laplace Transform and $g(t)$ is a partition function.
2. Advection in the matrix is neglected.
3. Flow velocity $\mathbf{V}(x)$ is spatially variable and at steady state, with advection dominated hydrodynamic transport whereby $\mathbf{J}(\mathbf{x}, t) = C(\mathbf{x}, t) \mathbf{V}(\mathbf{x})$.

Based on the first assumption, $F(C, S) \equiv g * \partial C / \partial t$ where “*” denotes convolution; in words, the sink-source term is defined as a convolution between the local rate of change of the mobile concentration C and the partition function g . The function g needs to be suitably selected for the problem at hand. For the simplest case of equilibrium retention, $g(t) = K'_d \delta(t)$ where $K'_d \equiv K_d(1 - \theta)\rho/\theta$ is a dimensionless partition coefficient, K_d [L³/M] is the partition coefficient, ρ [M/L³] is the density, and θ the porosity. First-order kinetic mass transfer is obtained if $g(t) = k_1 \exp(-k_2 t)$ where k_1 [1/T] is the forward and k_2 [1/T] backward rate, respectively; for $k_2 \rightarrow \infty$ with finite $k_1/k_2 \rightarrow K'_d$, the first-order and equilibrium models are equivalent in the limit.

3.1. Single Advection Trajectory

Because the Eulerian mass balance system (1) is assumed linear, it can readily be redefined for the solute flux. Taking advantage of the fluid mass balance in a stream tube, (1) can be transformed to one-dimensional Lagrangian mass balance equations for the solute discharge with units [M/T], with advective travel time τ [T] as the independent variable, following the steps of Cvetkovic and Dagan (1994). The result is

$$\frac{\partial \gamma_{ar}}{\partial t} + \frac{\partial \gamma_{ar}}{\partial \tau} = -\frac{\partial \gamma_r^*}{\partial t} = -\frac{\partial}{\partial t} \int_0^t \gamma_{ar}(t - \vartheta, \tau) g(\vartheta) d\vartheta \quad (2)$$

where γ_{ar} [1/T] denotes the normalized tracer discharge for an advection-retention process and γ_r^* [1/T] denotes the immobile tracer discharge as an auxiliary quantity. Pulse injection (of unit mass) is assumed as a baseline case. An integrodifferential formulation of multirate transport in rocks with the sink-source terms resembling the RHS of equation (2) was considered, for example, by Carrera et al. (1998).

Equation (2) can be solved to yield the conditional solution for γ_{ar} as

$$\gamma_{ar}(t, \tau) = \int_0^t \gamma_a(t - \vartheta - \tau) \gamma(\vartheta, \tau) d\vartheta = \gamma(t - \tau, \tau) \quad (3)$$

where

$$\gamma(t, \tau) = \mathcal{L}^{-1}[\exp(-\tau s \hat{g})] \quad (4)$$

is obtained by inverse Laplace Transform \mathcal{L}^{-1} , s is the Laplace Transform variable and $\gamma_a = \delta(t - \tau)$ since hydrodynamic transport is assumed by advection only. $\gamma(t, \tau)$ (4) is referred to as the retention time distribution (RTD) with particular significance for the implementation of the time domain random walk in advanced application tools for transport of radioactive chains (Painter et al., 2008; Painter & Mancillas, 2013; Trincherro et al., 2016).

The trajectory (or stream tube) conceptualization assumes that a tracer parcel consisting of, for example, molecules or ions, is advected and dispersed by kinetically controlled mass transfer. In other words, due to the exchange between the mobile and immobile zones, tracer molecules are temporarily trapped in the immobile zones, eventually returning to the mobile zone, again being trapped, with this process being repeated randomly until all molecules leave the system. If the advection scale of interest is denoted by L (e.g., length scale of a tracer test, or the extent of a discrete fracture), the total time a tracer molecule will spend over the distance L is $\tau + T$, where T is a *retention time*. This time quantifies how long a tracer particle will be immobilized along a trajectory with water travel time τ over a distance L . The RTD (4) is the probability density function (PDF) of T (Cvetkovic, 2017; Cvetkovic et al., 2016).

3.2. Retention in Crystalline Rocks

General formulations of g that can account for Fickian or non-Fickian diffusion has been presented in Cvetkovic (2017). In the following, we shall consider mass transfer controlled by Fickian diffusion as supported by available data. Hence, we consider the special case of a truncated power law form as presented in Cvetkovic (2017) with exponent 1/2:

$$\hat{g}(s) = \frac{1}{s\sqrt{T_1}} \left[\sqrt{\frac{1}{T_2} + s} - \frac{1}{\sqrt{T_2}} \right] \quad (5)$$

$$g(t) = \frac{1}{\sqrt{T_1 T_2}} \left(\text{Erf} \left[\sqrt{t/T_2} \right] - 1 \right) + \frac{e^{-t/T_2}}{\sqrt{\pi T_1} t} \quad (6)$$

where T_1 [T] is a characteristic retention (or trapping) time, and T_2 [T] is a characteristic return time that controls asymptotic behavior and the extent of the tailing. A g that is derived by explicitly solving for diffusion into a matrix can be shown to be exactly (5) and (6) for an infinite matrix ($T_2 \rightarrow \infty$), and approximately (5) and (6) for a finite matrix, where the associated parametric relationships have been identified by method of moments (Cvetkovic, 2017) (see Appendix A for a summary). Note that in Cvetkovic (2017) $k_1 \equiv 1/T_1$ and $k_2 \equiv 1/T_2$ where used and referred to as “rates” in view of their dimension [1/T].

With the retention process described as Fickian diffusion into a (un)limited matrix using (5) and (6), combining (4) and (5), and inverting, we obtain a closed-form expression for the RTD as

$$\gamma(T, \tau) = \frac{\tau}{2 T \sqrt{\pi T T_1}} \exp \left(-\frac{T}{T_2} + \frac{\tau}{\sqrt{T_1 T_2}} - \frac{\tau^2}{4 T T_1} \right) \quad (7)$$

which is the tempered one-sided stable (TOSS) density (Cvetkovic, 2011) with exponent 1/2; more general forms with the exponent different from 1/2 have been discussed elsewhere (Cvetkovic, 2017). In Appendix B we compare the RTD with different partition functions: using g (5), using g for two geometrical models of diffusion-controlled retention and using g for first-order exchange.

3.3. Statistical Representation of Retention

A moment generating function of the type (4) implies a compound Poisson process, whereby the retention time T can be expressed as

$$T(\tau) = \sum_i^{N(\tau)} \Delta T_i \quad (8)$$

where ΔT_i are independent and identically distributed random variables with a PDF $p(\Delta T_i)$, and $N(\tau)$ is distributed following a Poisson process with the mean conditioned on the water travel time as $\tilde{N} = \tau/T_1$

(Cvetkovic, 2017). The PDF of the underlying process ΔT_i is defined in the Laplace domain as $\hat{p} = 1 - s\hat{g} T_1$, for any suitable g ; inversion of \hat{p} with \hat{g} (6) yields

$$p(\Delta T_i) = \frac{\sqrt{T_1} e^{-\Delta T_i/T_2}}{2\Delta T_i \sqrt{\pi \Delta T_i}} + \delta(\Delta T_i) \left(1 + \sqrt{\frac{T_1}{T_2}} \right) \quad (9)$$

For an infinite matrix $T_2 \rightarrow \infty$ and (9) writes

$$p(\Delta T_i) = \frac{\sqrt{T_1}}{2\Delta T_i \sqrt{\pi \Delta T_i}} + \delta(\Delta T_i) \quad (10)$$

When a tracer particle is advected along a trajectory with τ , it will enter the matrix N times, distributed as a Poisson process with conditional mean $\bar{N} = \tau/T_1$. Once in the matrix, a particle will be immobilized for a random time with PDF p (9). In other words, p controls the tail of the BTC. In Appendix C we discuss briefly the comparison between our statistical representation and the one presented for first-order exchange by Andricevic and Fofoula-Georgiou (1991).

3.4. Multiple Trajectories: Advective Travel Time

A convenient and general model for capturing Fickian or non-Fickian features of hydrodynamic transport in tracer experiments with multiple random trajectories is the TOSS density for advective travel time $f_\tau(\tau)$ [$1/T$]; it is defined in the Laplace domain as (Cvetkovic, 2011)

$$\hat{f}_\tau(s; L) = \exp \left[\frac{1-\alpha}{\alpha \zeta^2} - \frac{\bar{\tau}^\alpha}{\alpha} \left(\frac{1-\alpha}{\zeta^2} \right)^{1-\alpha} \left(\frac{1-\alpha}{\zeta^2 \bar{\tau}} + s \right)^\alpha \right] \quad (11)$$

where $\bar{\tau}$ is the mean and ζ is the coefficient of variation of the advective (water) travel time τ . The exponent $0 < \alpha < 1$ defines the range of non-Fickianity for the hydrodynamic transport if $\alpha \neq 1/2$; $\alpha = 1/2$ yields the solution of the advection-dispersion equation for injection in the flux, or the inverse-Gaussian PDF. For $\alpha \rightarrow 0$, f_τ converges to the Gamma distribution, whereas for $\alpha \rightarrow 1$ plug flow is recovered as $f_\tau \rightarrow \delta(\tau - \bar{\tau})$.

3.5. Multiple Trajectories: Tracer Discharge

Multiple random trajectories capture key features of macroscopic transport. With f_τ quantifying field-scale advective transport along multiple, random trajectories, the expected tracer discharge Q [M/T] at distance L for pulse injection of mass M_0 is given by

$$Q(t, L) = M_0 h(t, L) = M_0 \int_0^\infty \gamma_{ar}(t, \tau) f_\tau(\tau) d\tau \quad (12)$$

Note that if finite injection rate is considered, Q would be obtained by a convolution. For unit tracer mass ($M_0 = 1$), the solution (12) is particularly simple when expressed in the Laplace domain:

$$\hat{h}(s, L) = \int_0^\infty e^{-s \tau(1+\hat{g})} f_\tau(\tau) d\tau \equiv \hat{f}_\tau[s(1+\hat{g})] \quad (13)$$

a result originally obtained by Villiermaux (1974), provided that the PDF f_τ can be expressed in the Laplace domain. Specific choices of $f_\tau(\tau)$ and $g(t)$ determine the nature of the transport-retention process. For g (5) and (6), the controlling parameters are the characteristic retention time T_1 and the characteristic return time T_2 that are understood to be suitably defined effective values, since in the general case T_1 and T_2 are spatially variable. The simplest transport case is mean advection subject to equilibrium sorption obtained by $f_\tau(\tau) = \delta(\tau - \bar{\tau})$ with $g(t) = (T_2/T_1)\delta(t) \equiv (k_1/k_2)\delta(t)$, where δ is a Dirac delta function.

Equation (13) with (5) and (11) provides a general transport model for advection-dispersion with retention that can be used for evaluating tracer tests with Fickian or non-Fickian hydrodynamic transport.

4. Retention Indicators and Regimes

The most important indicators of retention from a measured BTC in rocks are the normalized peak, the time of peak arrival, and the slope of the asymptotic tailing, as much as it is available prior to termination of a test. The asymptotic tailing from tracer tests in granite typically follows a $-3/2$ slope indicative of Fickian

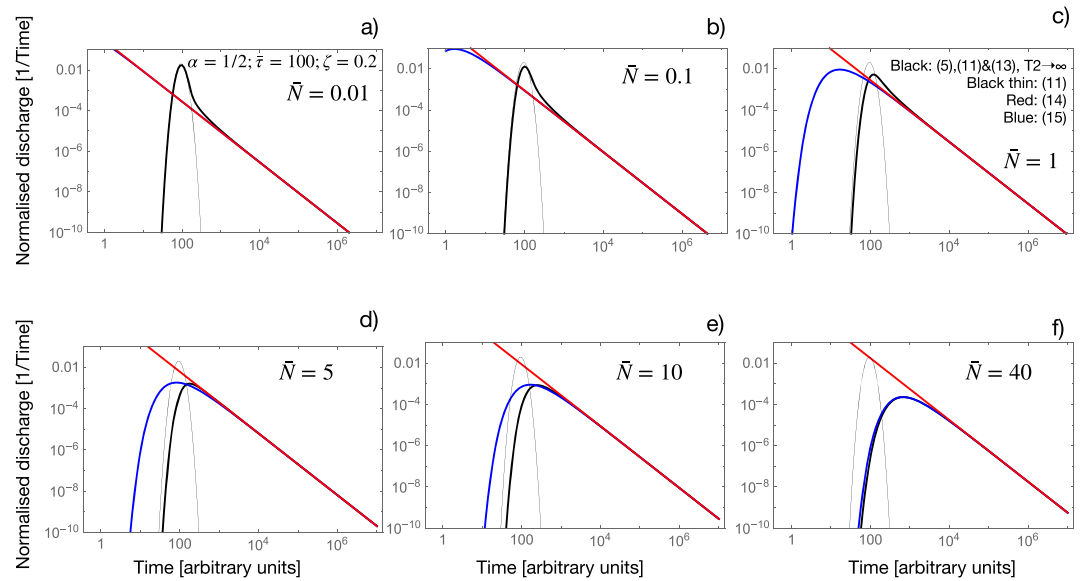


Figure 1. Generic cases that illustrate the range of the unconditional mean number of trapping events \bar{N} , between 0.01 (weak retention) and 40 (strong retention). The hydrodynamic transport is assumed with $\alpha = 1/2$ in (11) with $\bar{\tau} = 100$ and $\zeta = 0.2$: (a) $\bar{N} = 0.01$; (b) $\bar{N} = 0.1$; (c) $\bar{N} = 1$; (d) $\bar{N} = 5$; (e) $\bar{N} = 10$; (f) $\bar{N} = 40$. Time units are arbitrary. The black curves were obtained using equations (5), (11), and (13), the black thin curves were obtained using equation (11), the red curves were obtained using equation (14), and blue curves were obtained using equation (15). In all cases $T_2 \rightarrow \infty$.

diffusion-sorption in an unlimited matrix. If signs of a limited matrix (such as a rapidly declining tail) are not visible, then a bound for T_2 can be established based on the termination time. For instance, if the test was terminated at a time t_{term} with $-3/2$ slope, then one can state $T_2 \geq t_{\text{term}}$. Currently available evidence indicates that retention capacity in crystalline rock is sufficiently large for tracer tests; hence, we shall here assume $T_2 \rightarrow \infty$ and focus on T_1 . Our interest in this section is to understand if and how the key observable indicators of a BTC (normalized peak denoted by h^* , time of the peak arrival denoted by t^* and asymptotic tailing), can be used for inferring the characteristic retention time T_1 .

Following a tracer particle trapping random event, PDF of the time the particle will spend in the rock matrix is p (10). For average \bar{N} immobilization events, asymptotic transport can be approximated by the unconditional form of p denoted by \mathcal{P} and defined by

$$\lim_{t \rightarrow \infty} \gamma_{ar}(t, \tau) \approx \mathcal{P}(t) \equiv \bar{N} p(t) = \frac{\bar{N} \sqrt{T_1}}{2 \sqrt{\pi}} t^{-3/2} = \frac{\bar{\tau}}{2 \sqrt{\pi T_1}} t^{-3/2} \quad (14)$$

Expression (14) encapsulates the physics of the underlying trapping process: \mathcal{P} is proportional to the unconditional mean number of trappings $\bar{N} = \bar{\tau}/T_1$; however, the time spent in the matrix is proportional to $\sqrt{T_1}$; hence, the overall dependence of retention and its asymptotic behavior is controlled by the parameter group $\bar{\tau}/\sqrt{T_1}$ that can be calibrated from the BTC tail using (14). Note that a similar reasoning was used when computing the expected time in the mobile phase within a given time interval for a first-order exchange process, where the mean number of trapping events is multiplied by the mean time a tracer particle spends in the mobile phase following a trapping event (Andricevic & Foufoula-Georgiou, 1991, their equation (20)).

Based on the unconditional mean number of trappings $\bar{N} = \bar{\tau}/T_1$ (that may also be interpreted as a type of Damkohler number for the transport-retention process), one can identify the following three retention regimes:

- (a) *Decoupled regime*, $\bar{N} \leq 1$. Due to a relatively weak retention, hydrodynamic transport and retention are decoupled; that is, the bulk tracer discharge is controlled by hydrodynamic transport, and a distinct asymptotic tail due to diffusive mass transfer is observed.
- (b) *Partly coupled regime*, $1 < \bar{N} < 10$. The hydrodynamic transport and a moderate retention process are partly coupled.

Table 1
Estimates of the Retention Parameter T_1 for Different \bar{N} and for Fixed $\zeta = 0.2$

$\bar{N} = \bar{\tau}/T_1$ (-)	Estimated (actual) t_p (C4) (t_p^*) (T)	Actual T_1 (T)	Estimated T_1 (18) with $\bar{\tau} \approx t_p^*$ (T)	Estimated T_1 (18) with (19) (T)
0.01	100.17 (100)	10,000	10,000	157.5
0.1	101.67 (100)	1,000	1,000	105.3
1	116.67 (125.89)	100	158.7	53.2
2	133.33 (141.25)	50	100	33
3	150 (158.49)	33	84	25
4	166.67 (158.49)	25	62.5	13.8
5	183.33 (177.83)	20	63.3	12.5
6	200 (199.53)	16.7	66.2	12
7	216.66 (199.53)	14.3	56.8	6.9
8	233.33 (223.87)	12.5	62.5	7.6
9	250 (251.19)	11	70	8.7
10	266.67 (251.19)	10	63.3	5.4
40	766.67 (707.95)	2.5	125	0.37

(c) *Fully coupled regime*, $\bar{N} > 10$. The hydrodynamic transport and relatively strong retention are fully coupled (integrated).

The significance of the above retention regimes is that the strategy for inferring the characteristic retention time T_1 will depend on which of the regimes appears dominant for any given tracer test. Whereas the decoupled regime (a) is relatively easy to identify visually from a given BTC, regimes (b) and (c) cannot be identified visually. However, for practical reasons tracer tests are unlikely to be carried out in the fully coupled regime (c), since the duration of the tests would be prohibitive, in particular if one wishes to capture even a small part of the asymptotic tailing. Specifically, regime (c) would imply either a very long water travel time and/or strong retention with short T_1 , for example, because a strongly sorbing tracer is used. In practice, we do not anticipate tracer tests with $\bar{N} > 10$; summary of a number of nonsorbing tracer tests carried out in Swedish granite (to be discussed in a subsequent section) reveals an estimated maximum \bar{N} of around 3. For a tracer test with a sorbing tracer Na that will be discussed in the next section, $\bar{N} \approx 9$, with the test terminated after roughly 2 years and 4 months; such long tests however are rare.

To understand the significance and features of the retention regimes (a)–(c), consider the cases illustrated in Figure 1 which all assume relatively small macrodispersion with $\zeta = 0.2$ (consistent with a field-scale tracer test to be discussed in the following section). For the decoupled regime (a) (Figures 1a and 1b), we see that (14) yields the group $\bar{\tau}/\sqrt{T_1}$ from the asymptotic slope. Since in this regime, the time of peak arrival approximates relatively well $\bar{\tau}$, it is easy to infer T_1 from the calibrated value $\bar{\tau}/\sqrt{T_1}$. This is seen in Table 1 for cases $\bar{N} = 0.01, 0.1$ and even 1, where T_1 is estimated accurately for $\bar{N} = (0.01, 0.1)$, and up to a factor 2 for $\bar{N} = 1$ by this simple method.

Next, consider the partly coupled regime (b) illustrated in Figures 1c–1e. In this case, the unobservable RTD and the observable BTC exhibit roughly the same peak magnitude, that are shifted in time. The tail of the BTC can be used in this case for calibrating $\bar{\tau}/\sqrt{T_1}$ just as in Figures 1a and 1b; however, because retention is stronger in Figures 1c–1e, the tests would need to be run for a relatively long time in order to sufficiently capture the tailing. One way to circumvent the use of the tail for calibrating $\bar{\tau}/\sqrt{T_1}$ is to take advantage of the approximately same peak magnitude between the RTD and BTC in this regime. The RTD (4) writes

$$\gamma(T) = \frac{\bar{\tau} e^{-\frac{\bar{\tau}^2}{4T T_1}}}{2\sqrt{\pi T_1 T^3}} \quad (15)$$

Inserting the peak retention time denoted by T_p and derived in Appendix C as $T_p = \bar{\tau}^2/6T_1$ (C2), we deduce the peak of the RTD from (15) as

$$\gamma_p = \frac{3 T_1}{\bar{\tau}^2} \sqrt{\frac{6}{\pi e^3}} \quad (16)$$

If $\gamma_p \approx h^*$ with h^* being the observable (measured) peak of the BTC, (16) can be used to infer the parameter group $\bar{\tau}/\sqrt{T_1}$ by a simple expression

$$\frac{\bar{\tau}}{\sqrt{T_1}} = \frac{1}{\sqrt{h^*}} \sqrt[4]{\frac{2}{\pi} \left(\frac{3}{e}\right)^3} \quad (17)$$

Equation (17) reflects a fundamental coupling between hydrodynamic transport and retention. For upscaling transport it is critical to decouple $\bar{\tau}$ from T_1 even if only approximately. If the mean water travel time $\bar{\tau}$ can somehow be estimated from the measured BTC, T_1 can be inferred from (17) as

$$T_1 \approx \frac{\bar{\tau}^2 h^*}{\sqrt{\frac{2}{\pi} \left(\frac{3}{e}\right)^3}} \quad (18)$$

We suggest here two approaches for estimating $\bar{\tau}$ from the observed BTC:

- (i) The first approach is to approximate $\bar{\tau}$ with the observed (measured) peak arrival time denoted by t_p^* , that is, $\bar{\tau} \approx t_p^*$; this would be applicable in the decoupled regime (a), if the peak is relatively well defined and macrodispersion is not too large.
- (ii) The second method is more suitable in the partly coupled regime (b). The theoretical peak time of the BTC t_p (C4), can be used for estimating $\bar{\tau}$ by approximating t_p with the observable BTC peak t_p^* , that is, $t_p \approx t_p^*$, and utilizing (17) whereby

$$\bar{\tau} \approx t_p^* - \frac{1}{6 h^*} \sqrt{\frac{2}{\pi} \left(\frac{3}{e}\right)^3} \quad (19)$$

More detailed expressions that include the characteristic return time T_2 are given in Appendix C.

To test (18), we show estimates vs actual values in Table 1 for different \bar{N} , by generating hypothetical BTCs and underlying RTDs in the same manner as shown in Figure 1. As can be seen from the second column of Table 1, the approximation $t_p \approx t_p^*$ (C4) is reasonable, for the most part up to a few percent. The estimates of T_1 (18) with $\bar{\tau}$ obtained from (19) are accurate up to about a factor 2, which is a reasonable accuracy given the overall uncertainty in estimating retention properties (to be discussed in a subsequent section). We compare T_1 (18) with $\bar{\tau}$ estimated in two ways (last two columns in Table 1); in the partly coupled regime $1 < \bar{N} < 10$, T_1 (18) with $\bar{\tau}$ (19) provides a more reliable estimate (Table 1).

In the fully coupled regime (c) with $\bar{N} > 10$, the RTD and the BTC essentially coincide (Figure 1f), which implies that there is no means for estimating the characteristic retention time T_1 with any reliability (last row of Table 1). Whereas in the decoupled and partly coupled retention regimes (a) and (b), the use of multiple tracers (e.g., with different sorption properties) and/or use of different pumping rates for varying $\bar{\tau}$, can be taken advantage of for estimating in situ physical and sorption properties, for the fully coupled regime (c) even the use of multiple tracers with multiple flow conditions does not provide a means to separate T_1 from the group $\bar{\tau}/\sqrt{T_1}$. In this case, the only means of estimating T_1 is from independent information, either on the water travel time and/or from rock matrix samples.

Finally, the effect of macrodispersion is illustrated in Table 2 for a range of $0.1 \leq \zeta \leq 0.4$ with $\bar{N} = 5$ ($T_1 = 20$, $\bar{\tau} = 100$) and $\bar{N} = 10$ ($k_1 = 10$, $\bar{\tau} = 100$). Table 2 shows estimates of T_1 obtained using the two methods (i) and (ii) discussed above. As can be seen in Table 2, even for increasing dispersion, the two methods may provide reasonable bounds for T_1 in the case $\bar{N} = 5$, whereas for stronger retention with $\bar{N} = 10$, the estimates become less reliable with increasing ζ .

Table 2

Estimates of the Characteristic Retention Time T_1 for $\bar{N} = 5$ and $\bar{N} = 10$, With Different Levels of Macrodispersion as Quantified by the Water Travel Time Coefficient of Variation ζ

ζ (-)	$T_1 = 20$ (T)	$T_1 = 10$ (T)
0.1	(63.3, 15.7)	(63.3, 6.3)
0.2	(63.3, 12.5)	(63.3, 5.4)
0.3	(50, 6)	(50, 2)
0.4	(39, 2.8)	(34.7, 0.2)

Note. The values in the parentheses are T_1 obtained using equation (18) where $\bar{\tau}$ is estimated in two ways: The first value is T_1 (18) with $\bar{\tau} \approx t_p^*$ (i.e., the BTC peak is used as a proxy for the mean water travel time); the second value in the parentheses is T_1 (18) with $\bar{\tau}$ estimated using (19).

5. Illustration Examples

In this section, examples of field tracer tests performed in granite will be used to illustrate the approximate separation of $\bar{\tau}$ and T_1 , in the decoupled (a) and partly coupled (b) retention regimes, as the two regimes feasible in practice.

5.1. Decoupled Retention Regime

An experimental effort (Rock Matrix Retention Properties, REPRO) in ONKALO at Eurajoki (Finland) was initiated by Posiva Oy (Finland) to study matrix diffusion and infer retention properties in situ (Poteri et al., 2018a, 2018b); the tests are referred to as Water Phase Diffusion Experiments (WPDE). The two WPDE tests provide a unique fully controlled in situ/laboratory setup for addressing fundamental issues of radionuclide retention and transport. In spite of relatively well controlled flow, the WPDE tests exhibit complex hydrodynamic transport. Here we shall illustrate inference of the characteristic retention time T_1 under the decoupled regime (a), as discussed in the previous section.

The WPDE tests were performed in a $L = 1.905$ m long packed-off section of a drill hole. Two successive tracer tests were carried out using different flow rates. The first experiment (WPDE-1) was performed using flow rate of 20 $\mu\text{L}/\text{min}$. The second experiment (WPDE-2) used half of the flow applied in the WPDE-1, that is, 10 $\mu\text{L}/\text{min}$. The objective to use two different flow rates was that matrix diffusion is sensitive to the flow changes and a series of tests with different flow rates could provide a more reliable basis for inferring retention properties.

Advective delay in the tracer transport was reduced by minimizing the volume of the experimental hole section by a cylindrical dummy that was placed inside the drill hole, creating a 1.25 mm flow aperture between the drill hole wall and the dummy. A tracer test was performed by pumping water along the drill hole into the aperture. The created aperture is quite small compared to the roughness or variability in the caliber of the drill hole, which presumably resulted in a heterogeneous aperture field. Note that the most significant effect on the heterogeneity of the aperture is a slight eccentricity of the dummy. Tracer breakthrough times also indicated a channeled flow field. Details of the flow field appeared to be different between the two WPDE tests, even though the only change in the experiment was lowering of the flow rate.

A cocktail of tracers with different sorption properties (and to a much lesser extent different diffusion properties), were used in the tracer tests. Injected tracer cocktail in the WPDE-1 was composed of radioisotopes HTO (tritiated water), ^{22}Na , ^{36}Cl , and ^{125}I . All of these tracers were expected to be nonsorbing, except ^{22}Na , which was expected to be slightly sorbing. The WPDE-2 experiment included most of the tracers used in WPDE-1, but introduced a few additional more sorbing tracers. The tracer cocktail in WPDE-2 contained HTO, ^{22}Na , ^{36}Cl , ^{85}Sr , and ^{133}Ba . Common tracers in both tests are HTO, ^{22}Na , and ^{36}Cl ; however, the detection limit for ^{36}Cl turned out to be too high in the WPDE-1 tests such that the BTC tailing was not captured. Our present analysis will therefore include HTO and Na only. BTCs have been corrected for radioactive decay. The tracer source injection was of relatively short duration compared to the hydrodynamic transport; thus, the source terms in both tests can be treated as a Dirac delta function.

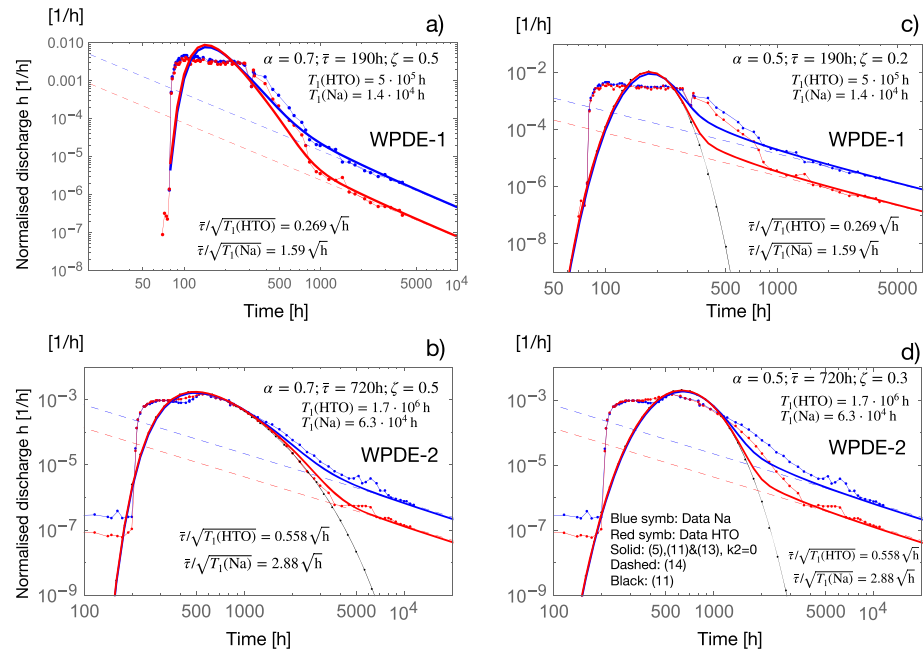


Figure 2. Modeled BTCs for the WPDE tests, assuming non-Fickian dispersion: (a) WPDE-1; (b) WPDE-2, and assuming Fickian dispersion: (c) WPDE-1; (d) WPDE-2. Calibrated parameters are indicated in the figure. The solid curves were obtained using equations 5, (11), and (13), dashed curves were obtained using equation (14), and black curves were obtained using equation (11). In all cases $T_2 \rightarrow \infty$.

Water particles move along trajectories of a complex and unknown flow field with tracer particles following the water by advection. The tracer particles are immobilized in the matrix (outward from the cylinder) with a conditional mean number of immobilization events τ/T_1 , and a PDF of immobilization time given by p (9). Results in the previous section point to the following evaluation strategy of the WPDE tests, summarized in two steps:

- Use TOSS (11) to calibrate $\bar{\tau}$, ζ and α for the initial hydrodynamic part of the BTC accounting for non-Fickian features;
- Insert inferred $\bar{\tau}$ into \mathcal{P} (14) and calibrate the slope to infer T_1 assuming a large rock matrix (i.e., $T_2 \rightarrow \infty$).

Note that the above steps are suitable for the WPDE tests because they fall into the decoupled retention regime (a). Our main interest is to infer the retention time T_1 for the two tracers, the nonsorbing HTO and sorbing Na. Due to complex flow, the bulk of the tracer discharge does not exhibit a clear peak; hence, we cannot use the simple expressions discussed in the previous section, but rather need to calibrate the advection-dispersion process. A total of three parameters need to be calibrated for hydrodynamic transport: the mean travel time $\bar{\tau}$, the coefficient of variation that quantifies dispersion ζ and the exponent α . For comparison, we shall also use the mean water travel time estimated from the flow rate Q [L^3/T] and the design volume V [L^3], as $\bar{\tau} = V/Q$.

The two experiments WPDE-1 and WPDE-2 differ by the flow rate magnitude. Clearly, the details of the advective-dispersive transport in the thin cylindrical annulus between the dummy and the rock matrix differ significantly in the two experiments. Furthermore, because the mass transfer is dependent on the flow, the conditions for retention are also different in the two tests.

The BTCs for both tests exhibit decoupling, that is, the initial hydrodynamic transport part that is roughly up to 700 hr in the WPDE-1, and to 3,000 hr in WPDE-2 test, followed by asymptotic tailing. Note that the initial hydrodynamic part of the BTC is confirmed in both tests by the overlap between the sorbing and nonsorbing tracer, Na and HTO. Furthermore, the hydrodynamic part of the BTC has a characteristic sharp front in both tests, followed by a plateau feature that does not resemble a Fickian advection-dispersion process. In fact the early arrival (steep rise of the BTC) in both WPDE-1 and WPDE-2 tests is due to some type of channeling, where certain parts of the volume act as stronger conduits. Our first task is to capture this regime as closely as possible by using the TOSS density (11) in order to infer $\bar{\tau}$ as accurately as possible.

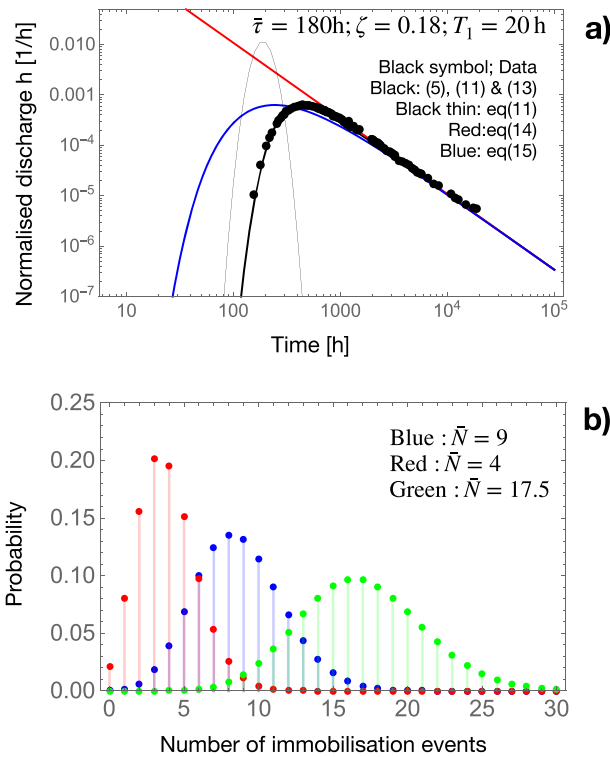


Figure 3. Evaluation of the C3 test of the TRUE Block Scale experiment (Cvetkovic et al., 2010) using the methodology proposed in the present work. (a) The normalized expected tracer discharge; (b) Poisson distributions of the immobilization events for $\tau = 80, 180,$ and 350 hr. The black thin curves were obtained using equation (11), red curves were obtained using equation (14), and blue curves were obtained using equation (15). In all cases $T_2 \rightarrow \infty$.

extensive laboratory program to determine retention properties from samples. The TRUE Block Scale experiments used cocktails of nonsorbing and sorbing tracers which resulted in total of 17 BTCs over Euclidian distances between 10 and 30 m. Low-sorbing Na was injected as a tracer in the C3 test. The flow path was between two boreholes approximately 30 m apart with estimated actual flow path length of around 40 m (see Cvetkovic et al. (2010) for details).

Applying \mathcal{P} (14) to the asymptotic part of the BTC, we infer the parameter group $\bar{\tau}/\sqrt{T_1}$ as $40 \text{ hr}^{1/2}$. With $\bar{\tau}/\sqrt{T_1} = 40 \text{ hr}^{1/2}$, the mean water travel time is inferred from (19) as $450-40^2/6 = 183 \text{ hr}$. With $\bar{\tau} = 183 \text{ hr}$ determined, we can infer T_1 as 20.8 hr from $\bar{\tau}/\sqrt{T_1} = 40 \text{ hr}^{1/2}$. The values of $\bar{\tau}$ and T_1 compare very closely to those obtained through significantly more elaborate means in Cvetkovic et al. (2010); see also Cvetkovic (2017) with a somewhat modified estimate of $\bar{\tau} = 180 \text{ hr}$ and $1/T_1 = 0.05 \text{ hr}^{-1}$.

Besides the BTC data, the different statistical representations of the transport process are shown in Figure 3. First, it is seen that dispersion is relatively low with a best estimate $\zeta = 0.18$ (Cvetkovic et al., 2010) (thin black curve in Figure 3a); calibration with the red curve yields the parameter group $\bar{\tau}/\sqrt{T_1} = 40 \text{ hr}^{1/2}$. The probability of the number of immobilization (trapping) events for the entire transport process is shown in Figure 3b. The blue symbols are the expected Poisson distribution, whereas the red and green symbols are Poisson distributions for the lower bound of water travel time approximated as 80 hr and the upper bound approximated as 350 hr, respectively, following the hydrodynamic transport (thin black line in Figure 3a).

To test the applicability of (18) with $\bar{\tau}$ estimated using (19), we extract from Table 3 in Cvetkovic (2017) $h^* = 0.0006315 \text{ hr}^{-1}$ and $t_p^* = 442 \text{ hr}$. Inserting these numbers into (19) yields $\bar{\tau} = 198 \text{ hr}$, while (18) yields $T_1 = 26.7 \text{ hr}$ which are close to previously obtained values (Figure 3). In this simple manner, from a single BTC with hydrodynamic transport and retention, $\bar{\tau}$ and T_1 are estimated without any calibration. Since (18) combined with (19) relies on the peak of the BTC only, a tracer test would not require monitoring of the tail;

The best fit of the BTCs is shown in Figure 2 for the two tracers HTO and Na in the two tests. The non-Fickian features of hydrodynamic transport are quantified by the exponent α in (11) that is in the range 0.7–0.8; the coefficient of variation in both cases is 0.5, whereas the mean travel time is calibrated as 190 hr in the WPDE-1 test, and 720 hr in the WPDE-2 test. If a Fickian regime is assumed, then $\alpha = 1/2$ in (11) and we recalibrate the coefficient of variation ζ in order to obtain the closest fit shown in Figures 2c and 2d; the main task was to capture as much as possible the sharp initial ascent of the BTCs. Comparing Figures 2a and 2c and Figures 2b and 2d, it is seen that the non-Fickian hydrodynamic transport using TOSS captures reasonably well the asymmetric shape of bulk part of both BTCs. If Fickian hydrodynamic transport is assumed, it does not capture these features and deviates more significantly from the data; further discussion and more detailed analysis of hydrodynamic transport in the WPDE tests are given in Poteri et al. (2018a, 2018b).

In spite of the difference in reproducing the measured BTCs, it is seen in Figure 2 that the asymptotic part of the BTCs which quantifies retention is not directly affected by assuming either Fickian or non-Fickian hydrodynamic transport. The slopes of the asymptotic BTCs are reproduced in both cases with the same T_1 values, also emphasized by the dashed lines representing PDF \mathcal{P} (14).

5.2. Partly Coupled Retention Regime

In this section we illustrate evaluation of a tracer test that falls into the partly coupled retention regime (b) with a relatively high estimated mean number of trappings (around 9). The tracer test in question is referred to as the C3 test, carried out as part of the TRUE Block Scale experiments in granite at the Äspö Hard Rock Laboratory (Oskarshamn, Sweden) at approximately 450 m depth (Cvetkovic et al., 2010). The rock volume that hosts the fracture network used in the experiments is approximately $100 \text{ m} \times 100 \text{ m} \times 50 \text{ m}$. The fractures used in the tracer tests were investigated using different nondestructive methods combined with an

in this case, the C3 tracer test could have been terminated after say 500–600 hr in stead of 20,000 hr and the same transport-retention parameters $\bar{\tau}$ and T_1 would have been inferred. This is clearly a relevant finding for more routine application of tracer tests in granite, that at least in some cases may significantly reduce the cost of in situ retention characterization.

6. Discussion

As shown in earliest studies, the geosphere performance for containing radionuclides or any other toxic substances, will critically depend on the retention process (de Marsily et al., 1977; Fried et al., 1987). Although hydrodynamic transport through rock fractures with diffusive mass transfer between mobile and immobile water are understood on the laboratory scale, retention is notoriously difficult to characterize or verify in situ. The only in situ verification or confirmation of a retention process is by means of tracer tests, preferably using a cocktail of tracers with different retention (e.g., sorption) properties such that at least the in situ ratios between the retention properties obtained in the laboratory can be verified (e.g., Cvetkovic, 2010a; Cvetkovic et al., 2007).

The key challenge in evaluating tracer tests is the process and parametric coupling between the hydrodynamic transport and retention. Insight into this coupling is most clearly revealed by the statistical representation of transport with retention. Whereas increasing unconditional mean number of trappings $\bar{N} = \bar{\tau}/T_1$ yields stronger retention, the time spent by a tracer particle trapped in the rock matrix decreases as $\sqrt{T_1}$; consequently, transport with retention is controlled by $\bar{N}\sqrt{T_1} = \bar{\tau}/\sqrt{T_1}$. In other words, the hydrodynamic and retention parameters are in principle inseparable. Yet for upscaling of transport, it is crucial to somehow separate T_1 from $\bar{\tau}$, since T_1 is a property of the fractured rock, whereas $\bar{\tau}$ also depends on boundary conditions for groundwater flow.

The novel form of a truncated power law partition function g (6), combined with the statistical representation of retention (Cvetkovic, 2017) enabled derivation of analytical expressions for estimating T_1 . However, inferring T_1 from the group $\bar{\tau}/\sqrt{T_1}$ is only the first step toward reliable upscaling. The next step is to identify how T_1 relates to the underlying material and structural properties of the fractured rock, which is important for reducing upscaling uncertainty. A specific question in this context is the dependence of T_1 on matrix porosity and diffusivity, and also on the fracture aperture. Fracture aperture is well known to vary spatially typically resulting in channeled flow. Mineralogical composition and microstructure of the rim zone are also known to vary spatially. The effect of these variabilities have been addressed on the level of single fractures (Cvetkovic, 2010b); the main research challenge is to understand effects of spatial variability in T_1 on the scale of discrete fracture networks. The currently only feasible approach to address spatial variability of T_1 in fracture networks is to assume that locally a Reynolds type of formulation for retention is applicable, in analogy with what is routinely assumed for the flow (Cvetkovic et al., 1999), and then use discrete fracture network simulations with realistic aperture variability in single fractures, to understand retention effects on larger scales. Addressing retention heterogeneity is an important research topic outside the scope of the present work. In the following, our goal will be to better understand underlying dependencies of T_1 on physical and sorption properties as a precondition for addressing retention heterogeneity. To this end tracer tests that we have evaluated in the past (Cvetkovic et al., 2007, 2010; Cvetkovic & Frampton, 2010) will be summarized and implications briefly discussed.

6.1. Physical Parameters

The starting point are expressions summarized in Appendix A for T_1 and T_2 in terms of underlying parameters, based on an idealized (rectangular channel) model. If a nonsorbing tracer is considered, then $K_d = 0$ and $R = 1$, whereby (A1) yields $1/T_1 = \omega^2 \theta^2 D_p$ where $\omega \equiv 2/e_{eff}$ [1/L] is an effective specific surface area with e_{eff} [L] being an effective aperture. The pore diffusivity D_p [L²/T] can be related to the matrix porosity θ and diffusivity in water D_w [L²/T] using Archie's law as $D_p = \theta^{m-1} D_w$ where m is the dimensionless Archie exponent. Assuming Archie's law and a rectangular channel configuration, matrix porosity and the effective aperture $e_{eff} = 2/\omega$ can be related using (A1) for a nonsorbing tracer ($R = 1$) as

$$e_{eff} = 2 \sqrt{\theta^{m+1} D_w T_1} \quad (20)$$

Thus, for an inferred T_1 and assumed m , the effective aperture and matrix porosity are related if the flow path is approximated as a rectangular channel. Note that typically θ , e_{eff} and m are all uncertain, only D_w is known. We shall illustrate in the following the implications of (20) for tracer tests in granite.

Table 3

Summary of the Inferred Characteristic Retention Time T_1 , the Mean Water Travel Time $\bar{\tau}$, and Distance L for Nonsorbing Tracer HTO if the WPDE, TRUE-1, and TRUE Block Scale (BS) Tests

Case	Test	Tracer	T_1 (hr)	$\bar{\tau}$ (hr)	L (m)
1	WPDE-2	HTO	1.7×10^6	720	2
2	WPDE-1	HTO	5×10^5	190	2
3	TRUE BS (C1)	$^{82}\text{Br}^-$	1100	15	28
4	TRUE BS (C2)	$^{186}\text{ReO}_4^-$	1100	200	80
5	TRUE BS (P2)	HTO	833	270	45
6	TRUE-1 (STT-2)	HTO	127	16	5
7	TRUE-1 (STT-1b)	HTO	83	5	5
8	TRUE-1 (STT-1)	HTO	59	7	5
9	TRUE BS (C3)	HTO	44	150	41
10	TRUE BS (P1)	$^{131}\text{I}^-$	14.8	12	20

Note. TRUE Stands for tracer retention understanding experiments. For TRUE Block Scale tests, calibrated ($\psi_0 \equiv 1/\sqrt{T_1}$) and $\bar{\tau}$ are taken from Table 1 in Cvetkovic et al. (2010). For TRUE-1 tests the calibrated ($t_d \equiv T_1$) and $\bar{\tau}$ were taken from Tables 4 and 5 in Cvetkovic et al. (2007); notation ψ_0 and t_d are used in the aforementioned references. The distance L values were taken from Table 5a (Cvetkovic & Frampton, 2010) for TRUE BS tests; for TRUE-1 the distance is 5 m (Cvetkovic et al., 2007). Note that for the TRUE BS tests, the distance relative to borehole distance was inferred by simulations and is approximate.

A series of tracer experiments were carried out in granite at the Äspö Hard Rock Laboratory (Oskarshamn, Sweden) between 1997–2007, with sorbing and nonsorbing tracers on scales with estimated flow path lengths in the range 5–80 m, and travel times in the range 5–270 hr (Cvetkovic et al., 2007, 2010). The characteristic retention time T_1 was calibrated using a full transport model, in the first series of tests (referred to as TRUE-1, scale 5 m) and the second series of tests (referred to as TRUE Block Scale, scale between 5 and 40 m).

In Table 3 we summarize the two key transport parameters calibrated in the TRUE tests: T_1 and the mean water residence time $\bar{\tau}$; included in Table 3 are also estimated flow path lengths. Besides the data for the TRUE tests, Table 3 also includes the values for the WPDE-1 and WPDE-2 tests; for ease of reference, values are listed in the descending order of T_1 , from the highest for the WPDE-2 test to the lowest for the TRUE BS P1 test.

In Figure 4, the relationship (20) is illustrated for T_1 given in Table 3. In the WPDE tests, matrix porosity and pore diffusivity are relatively well defined as $\theta = 0.006$, $D_p = 10^{-11}$ m²/s, and $D_w = 1.5 \times 10^{-9}$ m²/s (Poteri et al., 2018a), whereby Archie's law yields the exponent as $m = 1.98$. Using $\theta = 0.006$ and $m = 1.98$ in Figure 4a, we see that (20) yields e_{eff} around 3 mm for WPDE-2 and 1.6 mm for WPDE-1 test. Figure 4a illustrates the effect of the exponent m as a relatively mild change in the slope, where increasing m decreases the e_{eff} vs θ log-log slope. Note that an increasing m physically implies larger tortuosity in the rock matrix with zero tortuosity for $m = 1$. The presence of microfissures in the rim zone of granitic fractures will affect the tortuosity and hence the value of m . The tight and unaltered rock of the WPDE tests can therefore be expected to have a high tortuosity, that is, relatively large m , in addition to a low porosity.

Fracture rim zone in the TRUE test exhibited relatively strong alteration; hence, the overall retention as quantified by T_1 is significantly higher for TRUE tests compared to WPDE tests (Table 3). Consequently, matrix porosity in the TRUE tests is relatively large and also the tortuosity is expected to be lower with a comparatively low m . Using expression (20), the log-log dependence of e_{eff} on θ for high, medium, and low tortuosity as quantified by $m = \{1.8, 1.6, 1.4\}$ is illustrated in Figures 4b–4d. Given the scales involved and variability of matrix porosity in the rim zone, the effective aperture is highly uncertain. If a medium value of $m = 1.6$ is considered, and the matrix porosity is 1%, the range of effective apertures in all TRUE tests is 0.04–0.3 mm. If this range seems too low, $\theta = 1.5\%$ would yield a range of e_{eff} approximately 2 times

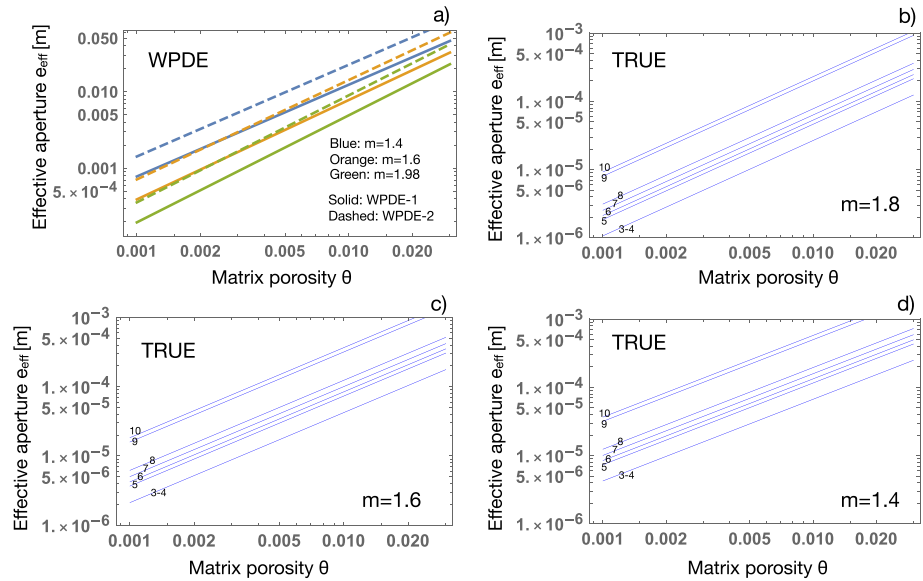


Figure 4. Theoretically possible range of effective aperture as a function of matrix porosity for the WPDE and TRUE tests with nonsorbing tracers: (a) WPDE tests with different Archie’s law exponent m ; (b) TRUE tests with $m = 1.8$; (c) TRUE tests with $m = 1.6$; and (d) TRUE tests with $m = 1.4$. The above curves were obtained assuming a simplified rectangular channel configuration with (A1) applicable. The values of T_1 are given in Table 3. Equation (20) is used for the illustration.

higher, that is, 0.07–0.6 mm. If the tortuosity is assumed to be lower with $m = 1.4$, then $\theta = 1.5\%$ yields the range of e_{eff} as 0.1–1 mm. Figure 4 clearly indicates that with T_1 calibrated, the inference of individual material and structural parameters relevant for retention (θ , m , e_{eff}) is by no means simple. Equation (20) may provide some indication or constraint on these individual parameters; however, (20) itself is uncertain since it assumes the flow path as a rectangular channel but also the applicability of Archie’s law.

6.2. Sorption Parameter

The inferred T_1 values for WPDE tests are summarized in Table 4. It is seen in Table 4 that T_1 estimates obtained by calibrating the full transport with (5), (11), and (13) differ by a factor 3 between WPDE-1 and

Table 4
Comparison Between In Situ T_1 for the Two WPDE Tests and T_1 Inferred From Sample Data, Where the Latter is Based on $\theta = 0.005\text{--}0.007$, $D_p = 0.7\text{--}1.3 \cdot 10^{-11} \text{ m}^2/\text{s}$ (Roughly Consistent With, e.g., Table 4-5 of Poteri et al., 2018a, 2018b), and $\omega = 1,000\text{--}2,000 \text{ m}^{-1}$

T_1 (hr)	HTO	Na	$T_1(\text{HTO})/T_1(\text{Na})$ $= R = 1 + \rho K_d/\theta$
WPDE-1			
T_1 (equation (14), $\bar{\tau} = V/Q = 344 \text{ hr}$)	1.6×10^6	47,600	34
T_1 (equations (5), (11), and (13) and Figure 2)	5×10^5	14,300	35
WPDE-2			
T_1 (equation (14), $\bar{\tau} = V/Q = 689 \text{ hr}$)	1.52×10^6	57,100	26.6
T_1 (equations (5), (11), and (13) and Figure 2)	1.6×10^6	62,500	27
Samples			
T_1 min	1.59×10^6		
T_1 max	111,000		540

Note. For $\omega = 2/e_{\text{eff}}$, $e_{\text{eff}} = 1\text{--}2 \text{ mm}$. See Appendix A for further details. The in situ T_1 was inferred in two ways: one by calibration of the entire BTC (solid red and blue curves in Figure 2), and the other by calibrating only the slope to infer the group $\bar{\tau}/\sqrt{T_1} [\sqrt{\text{hr}}]$ (dashed red and blue lines in Figure 2) and estimating $\bar{\tau} \approx V/Q$. $V = (r_b^2 - r_d^2)\pi L = 4.13 \cdot 10^{-4} \text{ m}^3$ where $r_b = 0.0565 \text{ m}$ is the borehole radius and $r_d = 0.054 \text{ m}$ is the radius of the dummy; the flow rates are $Q = 1.2 \cdot 10^{-6} \text{ m}^3/\text{hr}$ for WPDE-1, $Q = 0.6 \cdot 10^{-6} \text{ m}^3/\text{hr}$ for WPDE-2, and $L = 1.905 \text{ m}$ is the borehole test section length.

WPDE-2 tests. This uncertainty in T_1 is interpreted as a combination of the flow field effect, and the varying material retention properties over the exposed rock surface due to different flow regimes in the WPDE-1 and WPDE-2 tests. Table 4 includes T_1 estimated by calibrating $\bar{\tau}/\sqrt{T_1}$ using (14) with $\bar{\tau} = V/Q$ where V [L^3] is the design volume and Q [L^3/T] the experimental flow rate. It is seen from Table 4 that when using (14) with $\bar{\tau} = V/Q$, the estimated T_1 is the same for WPDE-2 and lower by about factor 3 for WPDE-1; interestingly, the estimated T_1 from WPDE-1 and WPDE-2 tests are almost the same in this case. Table 4 also includes T_1 as obtained from laboratory samples (last two rows), assuming an idealized flow path geometry; details for obtaining the sample T_1 are given in Appendix A.

Because WPDE tests included the nonsorbing tracer HTO and sorbing tracer Na, (A1) can be used to infer the retardation coefficient for Na in the rock matrix as

$$R \equiv 1 + \frac{\rho(1-\theta)K_d}{\theta} \approx \frac{T_1(\text{HTO})}{T_1(\text{Na})}$$

The resulting values of R are shown in Table 4 for WPDE-1 and WPDE-2 tests. As can be seen, the values from the two tests 27 and 35 are relatively close, differing by about 20%.

A summary of the sample data for different retention parameters is given in Poteri et al. (2018a, 2018b). Data were obtained using different techniques and on different samples; hence, a range of values was obtained. We shall use the laboratory values given in Poteri et al. (2018a), for example, in Table 4-5, accounting for the noted error range to obtain minimum and maximum values of the rate $T_1(\text{HTO})$ from laboratory samples. The most uncertain parameter is the flow-dependent specific surface area $\omega = 2/e_{\text{eff}}$ where e_{eff} is assumed in the range 1–2 mm. With these values, the sample estimates of $T_1(\text{HTO})$ differ by a factor 14 (Table 4). The retardation factor for Na R is determined using the best K_d estimate from Table 4-5 of Poteri et al. (2018a), with $\rho = 2,700 \text{ m}^3/\text{kg}$ and matrix porosity of 0.006.

As can be seen in Table 4, the inferred $T_1(\text{HTO})$ (Figure 2) falls within the uncertainty range for HTO; however, the inferred range for R as 27–35 is almost 20 times lower than R estimated from laboratory samples. Since the laboratory K_d was obtained using crushed rock, it is expected that this value is larger than the in situ K_d . Hence, we conclude that the impact of the flow field on retention, combined with sorption coefficient estimates using crushed rock, is the main source of uncertainty in predicting retention properties from laboratory samples.

The effect of the specific surface area in single fractures and fracture networks has been discussed elsewhere (e.g., Cheng et al., 2003; Cvetkovic & Frampton, 2012; Larsson et al., 2012; Wels et al., 1994); the flow dependence and the notion of the active specific surface area have also been discussed in the past (e.g., Cvetkovic & Frampton, 2010; Cvetkovic & Gotovac, 2014). In (7) as well as in (C1) and (17), τ and T_1 appear as $\tau/\sqrt{T_1}$ and are both related to the flow field through the aperture. The group $\tau/\sqrt{T_1}$ may be alternatively expressed as $\beta\kappa$ (Cvetkovic et al., 1999): the flow-related dependency for a fracture is contained in $\beta = \omega\tau$, whereas $\kappa \equiv \theta\sqrt{D_p R}$ depends on the material properties of the matrix. For a variable aperture, τ and ω are inseparable and defined as β (Cheng et al., 2003; Cvetkovic et al., 1999).

7. Conclusions

1. The unconditional $\bar{N} = \bar{\tau}/T_1$ is a key dimensionless parameter for identifying three possible retention regimes: (a) decoupled ($\bar{N} < 1$), (b) partly coupled ($1 < \bar{N} < 10$), and (c) fully coupled ($\bar{N} > 10$). For low to moderate macrodispersion, approximate expressions yield T_1 up to a factor 2 for $\bar{N} < 10$; the bound for \bar{N} decreases with increasing macrodispersion. For $\bar{N} > 10$, the coupling is too strong and no approximate expression can be derived for reasonable estimates of T_1 ; this case, however, is unlikely to be of interest in practice due to prohibitively long experimental time.
2. Applicability of T_1 (18) was verified based on data from two tracer tests, the WPDE test which falls in the decoupled regime (a), and C3 test which falls in the partly coupled regime (b). WPDE tests are characterized by complex hydrodynamic transport and a very low \bar{N} , while C3 exhibits relatively low macrodispersion and an unusually high \bar{N} of around 9; thus, the two tests may be considered as limiting cases. For WPDE, the proposed methodology yields robust in situ estimates of T_1 , and likewise for the C3 tests; in both cases, the obtained T_1 is comparable to around 20% with T_1 obtained using advanced calibration methods. The travel time coefficient of variation ζ that quantifies our best estimate of macrodispersion did not affect the estimates of $\bar{\tau}$ and T_1 in the WPDE or the C3 test.

3. Inferred T_1 values from eight TRUE tests with nonsorbing tracers as summarized in Table 3, show a factor 75 range, from 15 to 1,100 hr; the lowest value in the TRUE tests is still 450 times lower than the smallest value in the WPDE tests. These wide ranges in T_1 are mainly attributed to differences in effective apertures for tested flow paths which in the WPDE case are artificial and comparatively large, as well as to fracture alterations at the TRUE site that typically yield higher matrix porosity in the rim zone relevant for tracer test time scales. Figure 4 (or equation (20)) can be used for constraining or estimating possible ranges of the physical parameters controlling retention (such as θ and e_{eff}), assuming some level of idealized geometry of flow paths or aperture structure.
4. The tempered power law partition function (5)–(6) yields the RTD in form of the TOSS density controlled by the advective travel time τ and two characteristic times T_1, T_2 (equation (B5) in Table B1). TOSS RTD is consistent with the geometrical models for diffusion-controlled retention if the finite matrix extent is properly interpreted (Appendix B). For decreasing T_1, T_2 , the RTD for diffusion-controlled and first-order retention models attain a similar form.
5. A working hypothesis for evaluation of a typical tracer test in granite should be that it falls into regime (a) or regime (b). The tracer test data should as a first step be evaluated using both of the proposed methods for regimes (a) and (b) as described in section 5. Depending on the outcome, estimates of the significance or level of macrodispersion, as well as of which regime is most appropriate, should be possible. The next iteration should then use the formulas for regime (a) or (b). The relatively simple analytical tools for the full BTC as given in (13), (11), and (5) (with $T_2 \rightarrow \infty$ and $\alpha = 1/2$ (ADE) as default values), should be used for more comprehensive sensitivity analysis in order to test consistency of the inferred $\bar{\tau}$ and T_1 values. Finally, the evaluation outcome should be compared/corroborated using any independent information that is relevant and available.

The statistical representation of transport and retention in granitic rocks considered in this work is fully consistent with the underlying conceptualization of the state-of-the-art modeling tools for safety and performance assessment of hypothetical nuclear repositories (Painter et al., 2008; Painter & Mancillas, 2009; 2013; Selroos et al., 2013; Trincherio et al., 2016) thereby increasing overall confidence when using inferred parameters in such tools. Note that although for tracer tests the simplifying assumption $T_2 \rightarrow \infty$ is justified, for safety and performance assessment it is important that g (6) includes diffusion limitations with finite T_2 of possible relevance for long transport times; we have illustrated this point in Figure B2 of Appendix B using a realistic set of parameters with $\bar{\tau} = 10$ m/yr. The fact that the inverse-Gaussian distribution seems to be sufficient for reproducing hydrodynamic transport in the C3 test (Figure 3) is encouraging and in line with what has recently been found for highly heterogeneous porous media using detailed numerical simulations by Fiori et al. (2017) and Jankovic et al. (2017). These works have also demonstrated the significance of accurate mean plume movement estimates for robust predictions of nonreactive tracer transport, which is in line with our observation that accurate estimation of $\bar{\tau}$ is critical for inferring the characteristic retention time T_1 .

Further progress in reducing uncertainties when evaluating tracer tests in crystalline rock will be based on better understanding of the effects of retention heterogeneity, from microstructure, aperture fields, to local material properties that control the coupling between hydrodynamic transport and retention. Perhaps the biggest challenge in this context is providing more reliable descriptions of fracture roughness that to some degree account for the rock evolution, driven by coupled thermomechanical and hydrogeochemical processes.

Appendix A: Relating Characteristic Retention Times to Sample Data

The characteristic retention times T_1 and T_2 can be related to retention and flow properties only if a simplified flow path geometry is assumed; for a homogeneous rectangular channel it can be shown that (Cvetkovic, 2017)

$$T_1 = \frac{1}{\omega^2 \theta^2 D_p R} \quad ; \quad T_2 \sim \frac{R \Delta^2}{D_p} \quad (\text{A1})$$

where $\omega \equiv 2/e_{\text{eff}}$ [1/L] is a specific surface area, e_{eff} [L] is an effective aperture, D_p [L^2/T] is the pore diffusivity, $R = 1 + \rho(1 - \theta)K_d/\theta$ is the retardation coefficient in the rock matrix with ρ [M/L^3] being the rock density, θ [-] matrix porosity, K_d [L^3/M] is the sorption coefficient for the rock matrix and Δ [L] is the finite

extent of the rock matrix where retention takes place. Note that the actual expression for T_2 will depend on which boundary condition for diffusion in the matrix is assumed (Appendix B).

Coupled advection and retention in a fracture-matrix system with spatially variable properties in the fracture plane, has been presented in Cvetkovic et al. (1999). The key assumption of their work was that the Reynolds equations are applicable both for flow and diffusive mass transfer, whereby one-dimensional diffusion into the rock matrix is applicable locally at \mathbf{x} , with aperture $e(\mathbf{x})$, matrix porosity $\theta(\mathbf{x})$, sorption coefficient $K_d(\mathbf{x})$ and pore diffusivity $D_p(\mathbf{x})$. Under such conditions, hydrodynamic control of retention is quantified by

$$\beta(\tau) = \int_0^\tau \frac{2 dz}{e[\mathbf{X}(z; \mathbf{X}_0)]}$$

where $\mathbf{X}(t; \mathbf{X}_0)$ is the equation of an advection trajectory originating at $\mathbf{x} = \mathbf{X}_0$ at $t = 0$.

The assumption $\beta = \tau\omega \equiv 2\tau/e_{\text{eff}}$ implies that the flow path is simplified as a uniform rectangular channel of aperture e_{eff} . If the volumetric flow rate through the channel is Q and the width of a channel is W , water mass balance yields $\beta = 2WL/Q$ where L is the transport length. Thus, when flow paths are simplified as rectangular channels, we have two alternative expressions for β , either in terms of the water residence time and aperture, or the volumetric flow rate and flow path width, that is,

$$\beta = \tau\omega \equiv \frac{2\tau}{e_{\text{eff}}} = \frac{2WL}{Q} \quad (\text{A2})$$

or

$$\frac{1}{T_1} = \left(\frac{\beta\kappa}{\tau}\right)^2 = \left(\frac{2}{e_{\text{eff}}}\right)^2 \kappa^2 = \omega^2 \theta^2 D_p R = \left(\frac{2LW}{\tau Q}\right)^2 \theta^2 D_p R \quad (\text{A3})$$

consistent with (A1). Alternatively,

$$\bar{N} \equiv \frac{\tau}{T_1} = \frac{(\beta\kappa)^2}{\tau} = \left(\frac{2}{e_{\text{eff}}}\right)^2 \beta \kappa^2 = \left(\frac{2}{e_{\text{eff}}}\right)^2 \left(\frac{4LW}{Q}\right) \kappa^2 = \left(\frac{4LW}{e_{\text{eff}}Q}\right) \theta^2 D_p R \quad (\text{A4})$$

Note that the difference between a rectangular and cylindrical configurations of the actual WPDE tests is small in the present context (Poteri et al., 2018a).

Appendix B: RTD

We compare here different retention models for granitic rocks. Specifically, we compare the RTD in form of the cumulative distribution function (CDF), for two geometrical models with alternative boundary conditions (zero flux or zero concentration), the TOSS model as proposed in Cvetkovic (2017) and used in this work, and finally the first-order model. The interest in this comparison is to show consistent effects of the characteristic retention times T_1 and T_2 across models. In Table B1 we summarize four expressions for the RTD defined in the LT domain.

Factor 4 in the expressions for the geometrical models, can be explained as follows. For the zero concentration boundary condition, $\Delta/2$ is the extent of the matrix to the next fracture where water flows but no solute is transported. For the zero flux boundary condition, the extent of the matrix to the neighboring fracture is Δ , where both water and solute is transported; in fact, solute transport must be symmetric such that the diffusive solute flux is zero at $\Delta/2$. The different meaning of Δ for the two boundary conditions, together with highly idealized symmetric setup required to ensure either of the boundary conditions, clearly motivates the need for a generalized model without geometrical constraints, such as the TOSS model (Table B1).

The RTD complementary CDF (or CCDF) are illustrated in Figure B1 for the four models, and for four combinations of T_1 and T_2 ; in all cases $\tau = 1$. First, we observe that the two geometrical models are indeed consistent (compare red and red dashed curves); only a slight difference is observed prior to the asymptotic decline of the tail. Consistency between the TOSS model (black curve) and the geometrical models for all cases, indicates that TOSS provides a suitable representation of diffusion-controlled retention. The first-order model deviates significantly (blue curve); however, its overall qualitative behavior as affected by $k_1 \equiv 1/T_1$ and $k_2 \equiv 1/T_2$ is similar to the diffusion models. Note that the rate k_2 of the first-order model depends on the capacity of the immobile phase; hence, to obtain consistency in the tail termination with

Table B1
Four Models for the RTD [1/T], all Based on (4) With Four Different Partition Functions \hat{g}

Model	Equation in LT domain	Equation number
First-order	$\exp\left(-\frac{s \tau k_1}{s+4k_2}\right)$	(B2)
Geometrical, zero concentration at $\Delta/2$	$\exp\left\{-s \tau \sqrt{\frac{1}{T_1 s}} \left[\coth\left(\sqrt{4T_2 s}\right) - \sqrt{\frac{1}{4T_2 s}}\right]\right\}$	(B3)
Geometrical, zero flux at $\Delta/2$	$\exp\left[-s \tau \sqrt{\frac{1}{T_1 s}} \tanh\left(\frac{1}{2} \sqrt{4T_2 s}\right)\right]$	(B4)
TOSS	$\exp\left[\frac{\tau}{\sqrt{T_1}} \left(\frac{1}{\sqrt{T_2}} - \sqrt{\frac{1}{T_2} + s}\right)\right]$	(B5)

Note. For the first-order model $\hat{g} = k_1/(s + k_2)$ and for the two geometrical models the partition function \hat{g} is given by equations(7) and (8) in Cvetkovic (2017); the TOSS model is given in (5). We use $k_1 \equiv 1/T_1$ and $k_2 \equiv 1/T_2$.

the geometrical models, the rate k_2 also requires a factor 4 (Table B1) to account for the matrix extent $\Delta/2$. Also note that the first-order model drops as a step function strictly at $T = 0$. This drop can be computed as $1 - e^{-k_1}$; thus, in Figures B1a and B1b the drop is to 10^{-5} and in Figures B1c and B1d the drop is to 0.632. It is clear from Figure B1 that the reverse rate $k_2 = 1/T_2$ has exactly the same asymptotic impact for all models. With large k_2 , the tail termination is early in all models, for small k_2 the tail termination occurs later; the overall shape of the RTD CCDF is controlled by the magnitude of k_1 and is very different between diffusion-controlled and first-order models in all cases except when k_1 and k_2 are both relatively large.

The expression (B5) in Table B1 can be inverted to obtain a closed form solution for the RTD CDF as

$$\text{RTD CDF}(T) = \frac{1}{2} \left[1 + \operatorname{erf}\left(\frac{2T/\sqrt{T_2} - \tau/\sqrt{T_1}}{2\sqrt{T}}\right) + e^{2\tau/\sqrt{T_1 T_2}} \operatorname{erfc}\left(\frac{\tau/\sqrt{T_1} + 2T/\sqrt{T_2}}{2\sqrt{T}}\right) \right] \quad (\text{B1})$$

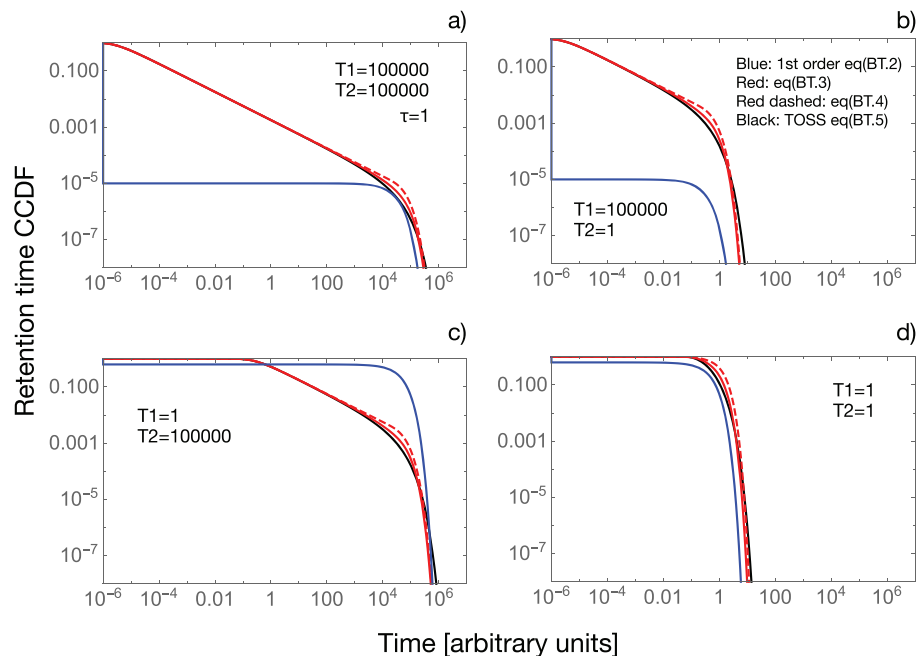


Figure B1. Complementary cumulative distribution functions (CCDF) of the RTD compared for four models of the partition function \hat{g} as summarized in Table B1 for (a) $T_1 = 10^5$, $T_2 = 10^5$; (b) $T_1 = 10^5$, $T_2 = 1$; (c) $T_1 = 1$, $T_2 = 10^5$; and (d) $T_1 = 1$, $T_2 = 1$. The expressions in Table B1 are PDFs of the retention time T , from which the CCDFs are readily obtained by numerical Laplace inversion.

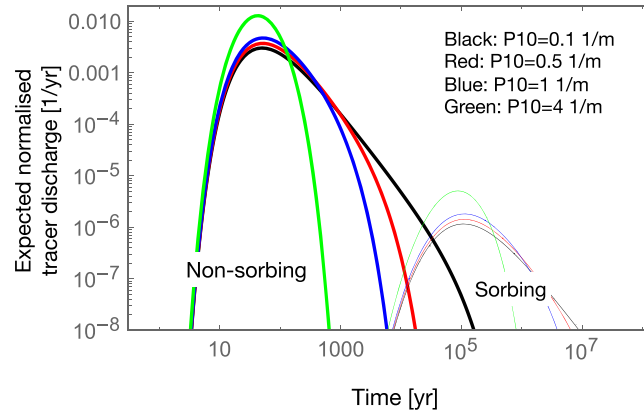


Figure B2. Effect of the characteristic return time T_2 on the expected normalized tracer discharge, for different fracture density P_{10} (m^{-1}). The following parameters have been used for a typical nonsorbing and sorbing tracer: Diffusivity in water $D_w = 0.053$ m^2/yr , matrix porosity $\theta = 0.01$, Archie's exponent $m = 1.8$, effective aperture $e_{eff} = 0.0004$ m , rock density $\rho = 2,700$ kg/m^3 and sorption coefficient $K_d = 0.01$ m^3/kg for the sorbing tracer. The characteristic return time was computed as $T_2 = R \Delta^2 / D_w \theta^{m-1}$ with the size of the rock matrix estimated as $\Delta \approx 1/P_{10}$ and R is the retardation coefficient; the characteristic retention time T_1 was estimated from (A1) where $\omega = 2/e_{eff}$ and $D_p = D_w \theta^{m-1}$. Mean advective travel time is assumed as $\bar{\tau} = 10$ m/yr .

which is equivalent in form to the solution by Ogata and Banks (1961) for the normalized cumulative discharge with detection in the flux.

Finally, we wish to illustrate the potential significance of a finite characteristic return time T_2 due to a limited rock matrix under realistic conditions. The simplest way to express fracture density (or intensity) is using the measure P_{10} [L] which quantifies the number of fractures per unit length of a borehole (Holmen & Outters, 2002). Its inverse $1/P_{10}$ [L] is a measure of the characteristic length between fractures, $\Delta \approx 1/P_{10}$.

In Figure B2 we illustrate the expected normalized tracer discharge obtained by numerical inversion of (13), with (5) and (11). The characteristic retention times T_1 and T_2 are estimated using realistic parameters for the Forsmark bedrock, summarized in the figure caption. The sensitivity parameter is the fracture density P_{10} as it has been shown to vary considerably with depth (Fox et al., 2007). It is seen in Figure B2 that the effect of T_2 clearly depends on the fracture density, and can be significant for $P_{10} > 1$; such values are observed for depths above 200 m (see e.g., Table 4-59 in Fox et al. (2007) for the Forsmark site).

Appendix C: Statistical BTC Indicators

Starting from the analytical expression for the RTD (7), the first derivative is

$$\gamma'(T) = \frac{\bar{\tau}}{8 T^3 \sqrt{\pi T} T_1} \left(\frac{\bar{\tau}^2}{T_1} - 6T - \frac{4T^2}{T_2} \right) \exp \left[-\frac{1}{4T} \left(\frac{\bar{\tau}}{\sqrt{T_1}} - \frac{2T}{\sqrt{T_2}} \right)^2 \right] \quad (C1)$$

The time of the RTD peak T_p can be obtained by solving the implicit equation $\gamma'(T_p) = 0$ as

$$T_p = \frac{T_1}{4} \left(\sqrt{9 + \frac{4\bar{\tau}^2}{T_1 T_2}} - 3 \right) \quad (C2)$$

which yields for the parameter group $\bar{\tau}/\sqrt{T_1}$

$$\frac{\bar{\tau}}{\sqrt{T_1}} = \sqrt{6 T_p + \frac{4 T_p^2}{T_2}} \approx \sqrt{6 T_p} \quad (C3)$$

relating $\bar{\tau}/\sqrt{T_1}$ to the unobservable peak time of the RTD T_p . We now wish to relate $\bar{\tau}/\sqrt{T_1}$ to the observable peak of the BTC, denoted by t_p^* .

For equilibrium sorption with a dimensionless sorption coefficient K'_d , the RTD is $\delta(t - K'_d \tau) \equiv \delta(t - t_R)$, in other words the peak of the RTD quantifies the shift in transport due to the retardation time $t_R = \tau K'_d$

relative to the water residence time τ . With analogous reasoning, the difference between the BTC peak t_p and the RTD peak T_p is the mean water travel time $\bar{\tau}$, that is,

$$t_p \approx \bar{\tau} + T_p = \bar{\tau} + \frac{\bar{\tau}^2}{6 T_1} = \bar{\tau} \left(1 + \frac{\bar{N}}{6} \right) \quad (C4)$$

The right-hand side of (C4) is obtained from (C2) in the limit $T_2 \rightarrow \infty$. This is an important result as it relates the retardation time $t_R = \bar{\tau} \bar{N} = \bar{\tau}^2 / T_1$ in (7) (that also controls the shape of \mathcal{P} (14)), to an approximation of the observable BTC peak, t_p^* , that is, $t_p \approx t_p^*$. Note that (C4) implies an apparent sorption coefficient as $\bar{N}/6$ and apparent retardation factor as $R_{app} = 1 + \bar{N}/6$, emphasizing the significance of the unconditional mean number of immobilization events \bar{N} for retention in rocks.

A statistical formulation of the first-order exchange process was presented by Andricevic and Foufoula-Georgiou (1991) (AF1991) using the renewal theory. The goal of their work was efficient numerical implementation of the first-order retention in transport codes; hence, the basic input for the analysis was the numerical time step Δt . AF1991 then compute the expected number of trappings over the time interval Δt , which differs from our \bar{N} computed here for the advective travel time τ . AF1991 determine the expected value of time spent in the mobile phase (denoted by Δt^*). In our case, the time spent in the mobile phase is τ and our main task is to compute the distribution of the time spent in the immobile phase during a given time step Δt (i.e., the RTD $\gamma(T, \tau)$ (4)). In spite of these differences in overall purpose as well as in the retention processes considered, the basic formulation of trapping events and the associated random times spent in mobile/immobile phase are similar.

References

Acknowledgments

This work was done as part of the Task Force on Modelling of Groundwater Flow and Transport of Solutes initiated and managed by the Swedish Nuclear Fuel and Waste Management Co (SKB). The first author gratefully acknowledges SKB support for participating in the Task Force program. We thank B. Gylling (Gylling GeoSolutions, USA) and A. Hautajärvi (AINS Group, Finland) for constructive comments that improved an early version of the manuscript. We are indebted to the WRR Associate Editor Olaf Cirpka (University of Tuebingen, Germany) and to the reviewer Tim Ginn (Washington State University, USA) for their constructive comments that significantly helped improve clarity of the originally submitted manuscript; appreciation is also extended to three anonymous reviewers who provided useful input. All computations were performed using Mathematica (R) software; the numerical Laplace Transform inversion was done using the method proposed by Abate and Valko (2004). The Mathematica notebook files that contain computations and all data can be downloaded from the Mendeley website (as <https://doi.org/10.17632/hbrxc5prtk.2>).

- Abate, J., & Valko, P. P. (2004). Multi-precision Laplace transform inversion. *International Journal for Numerical Methods in Engineering*, 60, 979–993. <https://doi.org/10.1002/nme.995>
- Andricevic, R., & Foufoula-Georgiou, E. (1991). Modeling kinetic non-equilibrium using the first two moments of the residence time distribution. *Stochastic Hydrology and Hydraulics*, 5, 155–171.
- Carrera, J., Benet, I., Medina, A., Galarza, G., & Guimera, J. (1998). On matrix diffusion: Formulations, solutions and qualitative effects. *Hydrogeology Journal*, 6, 178–190.
- Carslaw, H., & Jaeger, J. (1959). *Conduction of heat in solids*. New York: Oxford University Press.
- Cheng, H., Cvetkovic, V., & Selroos, J. (2003). Hydraulic control of retention in heterogeneous rock fractures. *Water Resources Research*, 39(5), 1130. <https://doi.org/10.1029/2002WR001354>
- Coats, K. H., & Smith, B. D. (1964). Dead-end pore volume and dispersion in porous media. *Society of Petroleum Engineers Journal*, 4, 73.
- Cvetkovic, V. (2010a). Diffusion-controlled tracer retention in crystalline rock on the field scale. *Geophysical Research Letters*, 37, L13401. <https://doi.org/10.1029/2010GL043445>
- Cvetkovic, V. (2010b). Significance of fracture rim zone heterogeneity for tracer transport in crystalline rock. *Water Resources Research*, 46, W03504. <https://doi.org/10.1029/2009WR007755>
- Cvetkovic, V. (2011). The tempered one-sided stable density: A universal model for hydrological transport? *Environmental Research Letters*, 6, 34008. <https://doi.org/10.1088/1748-9326/6/3/034008>
- Cvetkovic, V. (2017). Statistical formulation of generalized tracer retention in fractured rock. *Water Resources Research*, 53, 8736–8759. <https://doi.org/10.1002/2017WR021187>
- Cvetkovic, V., Cheng, H., Byegård, J., Winberg, A., Tullborg, E.-L., & Widestrand, H. (2010). Transport and retention from single to multiple fractures in crystalline rock at Äspö (Sweden): 1 Evaluation of tracer test results, effective properties and sensitivity. *Water Resources Research*, 46, W05505. <https://doi.org/10.1029/2009WR008013>
- Cvetkovic, V., Cheng, H., Widestrand, H., Byeård, J., Winberg, A., & Andersson, P. (2007). Sorbing tracer experiments in a crystalline rock fracture at Äspö (Sweden): 2. Transport modeling and effective parameter estimation. *Water Resources Research*, 43, W11421. <https://doi.org/10.1029/2006WR005278>
- Cvetkovic, V., & Dagan, G. (1994). Transport of kinetically sorbing solute by steady random velocity in heterogeneous porous formations. *Journal of Fluid Mechanics*, 265, 189–215.
- Cvetkovic, V., Fiori, A., & Dagan, G. (2016). Tracer travel and residence time distributions in highly heterogeneous aquifers: Coupled effect of flow variability and mass transfer. *Journal of Hydrology*, 543, 101–108. <https://doi.org/10.1016/j.jhydrol.2016.04.072>
- Cvetkovic, V., & Frampton, A. (2010). Transport and retention from single to multiple fractures in crystalline rock at Äspö (Sweden): 2 Fracture network flow and generic retention parameters. *Water Resources Research*, 46, W05506. <https://doi.org/10.1029/2009WR008030>
- Cvetkovic, V., & Frampton, A. (2012). Solute transport and retention in three-dimensional fracture networks. *Water Resources Research*, 48, W01209. <https://doi.org/10.1029/2011WR011086>
- Cvetkovic, V., & Gotovac, H. (2014). On the upscaling of chemical transport in fractured rock. *Water Resources Research*, 50, 5797–5816. <https://doi.org/10.1002/2014WR015505>
- Cvetkovic, V., Selroos, J. O., & Cheng, H. (1999). Transport of reactive tracers in rock fractures. *Journal of Fluid Mechanics*, 378, 335–356.
- de Marsily, G., Ledoux, E., Barbreaux, A., & Margat, J. (1977). Nuclear waste isolation: Can the geologist guarantee isolation? *Science*, 197, 4303.
- Fiori, A., Zarlenga, A., Jankovic, I., & Dagan, G. (2017). Solute transport in aquifers: The comeback of the advection dispersion equation and the first order approximation. *Advances in Water Resources*, 110, 349–359.
- Fox, A. P., Hermanson, J., & Öhman, J. (2007). La Pointe statistical geological discrete fracture network model: Forsmark modelling stage 2.2 (Report R-07-46). Stockholm, Sweden: Swedish Nuclear Fuel and Waste Management Co (SKB).
- Fried, S., Friedman, A. M., Atcher, R., & Hines, J. (1987). Retention of plutonium and americium by rock. *Science*, 196, 1087–1089.

- Hadermann, J., & Heer, W. (1996). The Grimsel (Switzerland) migration experiment: Integrating field experiments, laboratory investigations and modelling. *Journal Contaminant Hydrology*, 21, 87–100.
- Haggerty, R., McKenna, S. A., & Meigs, L. C. (2000). On the late-time behavior of tracer test breakthrough curves. *Water Resources Research*, 36, 3467–3479.
- Heer, W., & Smith, P. A. (1998). Modeling the radionuclide migration experiment at Grimsel. What have we learned? *Materials Research Society Symposium Proceedings*, 506, 663–670.
- Holmen, J. G., & Outters, N. (2002). Theoretical study of rock mass investigation efficiency (Technical Report TR-02-21). Stockholm, Sweden: Swedish Nuclear Fuel and Waste Management Co (SKB).
- Ittner, T., Torstenfelt, B., & Allard, B. (1990). Diffusion of strontium, technetium, iodine and cesium in granitic rock. *Radiochimica Acta*, 49, 101–106.
- Jankovic, I., Maghrebi, M., Fiori, A., & Dagan, G. (2017). When good statistical models of aquifer heterogeneity go right: The impact of aquifer permeability structures on 3D flow and transport. *Advances in Water Resources*, 100, 199–211.
- Johansson, H., Byegård, J., Skarnemark, G., & Skålberg, M. (1997). Matrix diffusion of some alkali- and alkaline earth-metals in granitic rock. *Materials Research Society Symposium Proceedings*, 465, 871–878.
- Johansson, M., Siitari-Kauppi, M., Tullborg, E. L., & Skålberg, M. (1998). Diffusion pathways in crystalline rock—Examples from Äspö diorite and fine-grained granite. *Journal of Contaminant Hydrology*, 35, 41–53.
- Larsson, M., Niemi, A., & Tsang, C. F. (2012). A study of flow-wetted surface area in a single fracture as a function of its hydraulic conductivity distribution. *Water Resources Research*, 48, 1944–1973. <https://doi.org/10.1029/2011WR010686>
- Neretnieks, I. (1980). Diffusion in the rock matrix: An important factor in radionuclide retention. *Journal of Geophysical Research*, 85(B8), 4379–4397.
- Ogata, A., & Banks, R. B. (1961). A solution of the differential equation of longitudinal dispersion in porous media (*Profl. Paper, No. 411-A*). Washington, DC: U.S Geological Survey.
- Painter, S., Cvetkovic, V., Mancillas, J., & Pensado, O. (2008). Power-law velocity distributions in fracture networks: Numerical evidence and implications for tracer transport. *Water Resources Research*, 44, W01406. <https://doi.org/10.1029/2007WR005944>
- Painter, S., & Mancillas, J. (2009). MARFA version 3.2.2 user's manual: Migration analysis of radionuclides in the far field SKB (*Report R-09-56*). Stockholm: Swedish Nuclear Fuel and Waste Management Co. (SKB).
- Painter, S., & Mancillas, J. (2013). MARFA user's manual: Migration analysis of radionuclides in the far field (*POSIVA Working Report 2013-01*). Helsinki, Finland: Posiva Oy.
- Poteri, A., Andersson, P., Nilsson, K., Byegård, J., Skålberg, M., Siitari-Kauppi, M., et al. (2018b). *The second matrix diffusion experiment in the water phase of the REPRO project: WPDE 2*. Finland, Posiva Oy, Olkiluoto.
- Poteri, A., Andersson, P., Nilsson, K., Byegård, J., Skålberg, M., Siitari-Kauppi, M., et al. (2018a). The first matrix diffusion experiment in the water phase of the REPRO project: WPDE 1 (*Posiva Working Report 2017-23*). Finland: Posiva Oy, Olkiluoto.
- Reimus, P., & Callahan, T. J. (2007). Matrix diffusion rates in fractured volcanic rocks at the Nevada Test Site: Evidence for a dominant influence of effective fracture apertures. *Water Resources Research*, 43, W07421. <https://doi.org/10.1029/2006WR005746>
- Reimus, P., Pohll, G., Mihevc, T., Ghapman, J., Haga, M., Lyles, B., et al. (2003). Testing and parametrizing a conceptual model for solute transport in a fractured granite using multiple tracers in a forced-gradient test. *Water Resources Research*, 39(12), 1356. <https://doi.org/10.1029/2002WR001597>
- Robinet, J. C., Sardini, P., Delay, F., & Hellmuth, K. H. (2008). The effect of rock matrix heterogeneities near fracture walls on the residence time distribution (RTD) of solutes. *Transport in Porous Media*, 72, 393–408.
- Sardini, P., Robinet, J. C., Siitari-Kauppi, M., Delay, F., & Hellmuth, K. H. (2007). Direct simulation of heterogeneous diffusion and inversion procedure applied to an out-diffusion experiment. Test case of Palmottu granite. *Journal of Contaminant Hydrology*, 93, 21–37.
- Selnert, E., Byegård, J., & Widestrand, H. (2007). Forsmark site investigation. Laboratory measurements within the site investigation e for the transport properties of the rock (Final report. Report P-07-139): Swedish Nuclear Fuel and Waste Management Co.(SKB).
- Selroos, J. O., Cheng, H., Painter, S., & Vidstrand, P. (2013). Radionuclide transport during glacial cycles: Comparison of two approaches for representing flow transients. *Physics and Chemistry of the Earth, Parts A/B/C*, 64, 32–45.
- Shapiro, A. (2001). Effective matrix diffusion in kilometer-scale transport in fractured crystalline rock. *Water Resources Research*, 37, 507–522.
- Trincherio, P., Painter, S., Ebrahimi, H., Koskinen, L., Molinero, J., & Selroos, J. O. (2016). Modelling radionuclide transport in fractured media with a dynamic update of Kd values. *Computers and Geosciences*, 86, 55–63. <https://doi.org/10.1016/j.cageo.2015.10.005>
- Tsang, C. F., & Neretnieks, I. (1998). Flow channeling in heterogeneous fractured rocks. *Reviews of Geophysics*, 36(2), 275–298. <https://doi.org/10.1029/97RG03319>
- Trincherio, P., Painter, S., Ebrahimi, H., Koskinen, L., Molinero, J., & Selroos, J. O. (2016). Modelling radionuclide transport in fractured media with a dynamic update of Kd values. *Computers & Geosciences*, 86, 55–63. <https://doi.org/10.1016/j.cageo.2015.10.005>
- Villiermaux, J. (1974). Deformation of chromatographic peaks under the influence of mass transfer phenomenon. *Journal of Chromatographic Science*, 12, 822–831.
- Wels, C., Smith, L., & Vandergraaf, T. T. (1994). Influence of specific surface area on transport of sorbing solutes in fractures: An experimental analysis. *Water Resources Research*, 32, 1943–1954.
- Widestrand, H., Byegård, J., Cvetkovic, V., Tullborg, E.-L., Winberg, A., Andersson, P., & Siitari-Kauppi, M. (2007). Sorbing tracer experiments in a crystalline rock fracture at Äspö (Sweden): 1. Experimental results and micro-scale characterization of retention properties. *Water Resources Research*, 43, W10413. <https://doi.org/10.1029/2006WR005277>